CD11c-expressing microglia are transient, driven by interactions with apoptotic cells

Nathaniel Ghena[1,2] ¶, Sarah R Anderson[1] ¶, Jacqueline M Roberts[1], Emmalyn Irvin[1], Joon Schwakopf[1], Alejandra Bosco[1], and Monica L Vetter[1,2] *

[1.] Department of Neurobiology, University of Utah School of Medicine

[2.] Interdepartmental Program in Neuroscience, University of Utah

¶ These authors contributed equally to this work

* Corresponding author

E-mail: monica.vetter@neuro.utah.edu

Abstract:

Microglia, the parenchymal macrophage of the central nervous system serve crucial remodeling functions throughout development. Microglia are transcriptionally heterogenous, suggesting that distinct microglial states confer discrete roles. Currently, little is known about how dynamic these states are, the cues that promote them, or how they impact microglial function. In the developing retina, we previously found a significant proportion of microglia express CD11c (Integrin αX, complement receptor 4, *Itgax*) which has also been reported in other developmental and disease contexts. Here, we sought to understand the regulation and function of CD11c+ microglia. We found that CD11c+ microglia track with prominent waves of neuronal apoptosis in postnatal retina. Using genetic fate mapping, we provide evidence that microglia transition out of the CD11c state to return to homeostasis. We show that CD11c+ microglia have elevated lysosomal content and contribute to the clearance of apoptotic neurons, and found that acquisition of CD11c expression is, in part, dependent upon the TAM receptor Axl. Using selective ablation, we found CD11c+ microglia are not uniquely critical for phagocytic clearance of apoptotic cells. Together, our data suggest CD11c+ microglia are a transient state induced by developmental apoptosis rather than a specialized subset mediating phagocytic elimination.

Introduction:

Microglia, the parenchymal macrophage of the central nervous system (CNS), serve crucial remodeling functions throughout development, including the refinement of circuits and cell elimination (1, 2). Single-cell analysis has revealed that microglia are transcriptionally heterogeneous during development (3, 4). However, the cues that produce specific states, the functional role(s) associated with these states, and how dynamic and reversible these states are not well understood.

46 The developing retina is an ideal CNS system to link well-characterized developmental events with
47 microglial properties and function. We previously found that murine retinal microglia gene expression
48 is heterogeneous and dynamic throughout development (5, 6). Notably, we showed that a majority of
49 microglia early in postnatal retina express CD11c (Integrin αX, complement receptor 4, *Itgax*) and
50 were remarkably similar to CD11c-expressing (CD11c+) microglia of the developing and diseased
51 brain (6, 7). By single-cell RNA sequencing, we found heterogeneity in CD11c+ microglia, but all
52 CD11c+ microglia expressed genes associated with phagocytosis and lysosomal function (6). In the
53 developing CNS, CD11c+ microglia predominantly reside in white matter tracts (8-10) and have
54 dynamic regional density changes over development in brain and spinal cord (11). CD11c+ microglia
55 are increased in diverse disease states. CD11c is a marker of disease-associated microglia (DAM,
56 MgND), enriched around Aβ plaques in Alzheimer's disease (12, 13). The appearance of CD11c+
57 microglia in these diverse contexts raises questions regarding their regulation and function. To
58 address this, we sought to understand the developmental cues and roles of CD11c+ microglia in
59 developing retina.
60 We previously showed a link between apoptosis and CD11c-expression, as *in vivo* loss of
61 developmental apoptosis dramatically reduced the proportion of CD11c+ retinal microglia and
62 expression of phagocytic genes (6). Consistent with this, microglia upregulate CD11c and coexpress
63 Osteopontin (OPN) in response to the engulfment of apoptotic neurons in cell culture (14). In addition,
64 CD11c+ microglia within developing white matter tracts engulf oligodendrocytes (9, 15), suggesting
65 that CD11c+ microglia may play a key role in phagocytosis. We found that the proportion of CD11c+
66 microglia over retina development is dynamic, which raises the question of whether developmental
67 CD11c+ microglia represent a transient state associated with cell death and phagocytic function, and
68 whether these cells mediate a specialized role in engulfment.
69 Here, we find that CD11c+ microglia density in the retina coincides with waves of neuronal apoptosis,
70 that CD11c+ microglia predominately associate with dying neurons and are phagocytic. Through

genetic fate mapping, we find that CD11c+ microglia shift to CD11c- state after periods of developmental apoptosis. Additionally, we find that loss of Axl reduced the proportion of CD11c+ cells, implicating Axl-mediated recognition of apoptotic cells in driving CD11c+ microglial state. Using selective depletion, we find both CD11c+ and CD11c- microglia contribute to the timely clearance of apoptotic neurons in the retina. Altogether, these data suggest that CD11c+ microglia in the developing nervous system represent a dynamic population driven by phagocytic interactions with apoptotic cells.

Results

CD11c-microglia coincide with developmental cell death

We previously found an increased proportion of CD11c+ microglia in postnatal retina compared to embryonic or adult stages, partially dependent on developmental cell death (6). We therefore hypothesized that CD11c+ microglia arise in response to interactions with apoptotic cells. To test this, we first utilized CD11c-DTR/GFP transgenic mice, in which the *Itgax* promoter (CD11c) directs expression of a diphtheria toxin receptor-enhanced green fluorescent protein fusion protein (DTR/GFP) (16). We confirmed via flow cytometry that GFP expression accurately correlates with surface expression of CD11c protein in naïve CD11c-DTR/GFP mouse retinas (Supplementary Figure 1A). Next, we quantified the density of CD11c+ cells by GFP expression and found the density of CD11c+ cells peaks between postnatal (P) 5 and P10, and drops by P30 (Figures 1A, B). Using complement component 1q (C1q), which specifically and stably labels microglia in the developing retina (5), we confirmed CD11c-GFP+ cells are microglia and peak at P5 consistent with our previous single-cell sequencing data (Figure 1C, D; (6)). Morphologically, CD11c+ microglia become more complex over the course of development, similar to non-CD11c microglia (Figure 1E; (6)). By analyzing retinal cross-sections, we found that CD11c-GFP+ microglia distribute primarily in the

95 ganglion cell layer (GCL) until P3, followed by a shift to the inner nuclear layer (INL) at P7,
96 spatiotemporally tracking with developmental cell death (Figures 1F, G; (17, 18)). Altogether, CD11c+
97 microglia track with periods of cell death across development and within specific retinal subregions.
98
99 **Figure 1. CD11c+ microglia density and localization track with periods of apoptosis.** (A) *Left* –
100 schematic of retinal flat mount depicting where analysis was conducted, with dorsal leaf outlined in
101 dashed yellow box. *Right* – max projected confocal images of CD11c-GFP+ cells in the dorsal leaf of
102 retinal flat mounts at postnatal days (P) 0, 7, and 30. Optic nerve head outlined in dashed white line.
103 Scale bar, 100μm. (B) Densities of CD11c-GFP+ cells from retinal flat mount across embryonic and
104 postnatal ages. Data are presented as means ± SEM (2-3 animals age). One-way ANOVA F(9,17)
105 =18.87 P<.0001. (C) Representative Max projected confocal image of C1q+ (red) and CD11c-GFP+
106 (green) microglia at P5. Scale bar 50μm. (D) Proportion of CD11c-GFP+ retinal microglia from retinal
107 flat mounts at embryonic day (e) 16.6, P0, P5, P12, and P30. Data are presented as mean ± SEM (2-
108 3 animals/age. One-way ANOVA F(4, 5) =15.76 *P=.0049* and Tukey's multiple comparisons. *$P \leq .05$,
109 *NS* =no significance. (E) Max projected confocal images of individual CD11c-GFP+ microglia in
110 retinal flat mounts from embryonic day 16.5 (e16.5) through postnatal day 30 (P30). Scale bar at
111 10μm. (F) Confocal images of retinal cross sections from CD11c-DTR/GFP transgenic mice at P0,
112 P3, P7, and P30. CD11c-GFP (Magenta); Hoechst (blue). For P0/3, brackets segment retinal layers,
113 gray – nerve fiber layer and ganglion cell layer (NFL/GCL), purple – inner plexiform layer (IPL), and
114 teal – neuroblastic layer (NbL). P7/P30, gray – nerve fiber layer and ganglion cell layer (NFL/GCL),
115 purple – inner plexiform layer and inner nuclear layer (IPL/INL), and blue – outer plexiform layer
116 (OPL) for P7 and P30. Scale bar, 100μm. (G) Percentage of CD11c-GFP+ microglia across all retinal
117 layers at P0, P3, P7, and P30 (n = 2 animals). Data are presented as means ± SEM.
118

119 ## Microglia transition out of the CD11c state

120 Since we found the proportion of CD11c-GFP+ microglia shifts throughout retina development, we
121 predict CD11c+ microglia are a transient state rather than a stable population. To test this, we
122 performed lineage-tracing to identify microglia that have expressed CD11c by utilizing CD11c-
123 Cre/GFP transgenic mice (19) crossed with Rosa-Ai14 tdTomato reporter mice (20) (Figure 2A). With
124 this strategy, cells actively expressing CD11c will express GFP while cre-mediated recombination
125 stably marks cells that previously expressed CD11c (Figure 2A). Therefore, cells expressing CD11c
126 (CD11c-active) would be GFP^+ $tdTomato^+$ or $GFP^+tdTomato^-$, while cells that previously expressed
127 CD11c (CD11c-lineage) would be GFP^- $tdTomato^+$, and cells that never expressed CD11c (CD11c-
128 negative) would be GFP^- $tdTomato^-$ (Figure 2A). Using flow cytometry, we found that the proportion of
129 microglia CD11c-active matched our previous quantification of CD11c+ microglia at P5 and P30
130 (~50% and <20%, respectively) while surprisingly, the majority of the remaining microglia were
131 CD11c-lineage. This suggests that nearly all postnatal retinal microglia have either previously express
132 or are currently expressing CD11c (Figure 1E; Figure 2B). Interestingly, the proportion of cells
133 marked as CD11c-lineage increased from P5 to P30 in a manner proportional to the reduction of
134 CD11c-active cells (Figure 2B), further evidence that CD11c-expression is transient and CD11c+
135 microglia convert to non-CD11c microglia. The P5 CD11c-active microglia population appeared more
136 phagocytic than the CD11c-lineage microglia at P5 as they had higher CD68 area, were more likely to
137 have phagocytic cups, and had more cups per microglia (Figure 2C – F). Bulk RNA-sequencing on
138 sorted P5 retinal microglia comparing CD11c-active and CD11c-lineage microglia confirmed that
139 CD11c-active have higher expression of genes associated with phagocytosis and remodeling states
140 *(Lamp1, Lyz2, CD68*) while CD11c-lineage have higher expression of homeostatic genes (*P2ry12,*
141 *Tgfbr1, Tmem119*) (Figure 2G). Altogether, these findings suggest that CD11c+ microglia are more
142 phagocytic and are not a stable subset, but shift to a non-CD11c state after resolution of periods of
143 developmental apoptosis.
144

145 **Figure 2. CD11c+ microglia are a dynamic state.** (A) Cartoon depiction of CD11c lineage tracing
146 strategy crossing CD11c-Cre/EGFP mice with Rosa-Ai14 tdTomato and the analysis performed at P5
147 and P30. (B) The proportion of microglia at P5 and P30, comparing microglia that are CD11c-active
148 (GFP+tdTomato+/total microglia), CD11c-lineage (GFP-tdTomato+/total microglia), and CD11-
149 negative (GFP-tdTomato-/total microglia) by flow cytometry. (C) Max Projected confocal image from
150 P5 CD11c-Cre$^{EGFP/+}$; Rosa$^{tdTomato/+}$ retinal flat mount. Insets ‘ CD11c-Active (gold box) and “ CD11c-
151 Lineage (pink box) microglia. CD68 (white), CD11c-Active (GFP, green), CD11c-Lineage (tdTomato,
152 red). Scale bar, 50μm. (D) Quantification of CD68 area in CD11c-Active and CD11c-Lineage
153 microglia at P5 (n=2 animals, 30 CD11c-Lineage cells and 50 CD11c-Active cells) ± SEM. Mann-
154 Whitney test ****P <.0001. (E) The proportion of CD11c-active and CD11c-lineage microglia with
155 phagocytic cups at P5 (n=2 animal) ± SEM. Unpaired t test ***P <.001. (F) Quantification of number
156 of phagocytic cups in CD11c-Active and CD11c-Lineage microglia at P5 (n=2 animal, 30 CD11c-
157 Lineage cells and 50 CD11c-Active cells) ± SEM. Unpaired t-test ***P <.001. (G) Bar graphs of RNA-
158 seq read counts for (top) genes with increased counts in CD11c-active and (bottom) genes with
159 decreased counts in CD11c-lineage.
160

161 CD11c-microglia phagocytose apoptotic cells and are regulated by Axl
162 signaling

163 Since we observed CD11c-expression in microglia to be transient, coinciding with periods of
164 developmental apoptosis, we asked whether CD11c+ microglia interacted with dying neurons *in vivo.*
165 At P3, during peak retinal ganglion cell (RGC) developmental apoptosis, we found CD11c-GFP+
166 microglia interacted with and engulfed apoptotic RGCs, as co-labeled by activated caspase 3 (CC3+)
167 and RGC marker RNA-binding protein with multiple splicing (RBPMS), with most CD11c-GFP+
168 microglia directly interacting with RBPMS+CC3+ cells (~70%; Figures 3A, B). Immunostaining for
169 lysosomal marker CD68 and microglial marker C1q, we found that the higher CD11c-GFP expression

170 correlated with elevated levels of CD68 and an enlarged amoeboid morphology, consistent with
171 increased lysosomal content and phagocytic/digestion activity (Figure 3C – E). This suggests that
172 CD11c-expression is driven by recent interactions and/or engulfment of apoptotic cell bodies.
173 Since exposure to apoptotic neurons increases CD11c-expression (6, 14, 21), we asked which
174 recognition pathways may be involved. Using flow cytometry, we analyzed genetic knockouts (KOs)
175 of receptors previously implicated in the recognition and phagocytosis of apoptotic neurons, namely
176 fractalkine receptor (CX3CR1, (22)), integrin receptor complement receptor 3 (CD11b/CR3, (23)), and
177 TAM receptors Mer and Axl (24, 25) (Figure 3F, Supplementary Figure 2A – F). While we previously
178 found that apoptotic RGC clearance was dependent on CR3 and Mertk (5), here we found that the
179 proportion of CD11c+ microglia was significantly reduced in both Axl KO and Mertk/Axl double KOs,
180 with approximately half the percentage of retinal microglia expressing CD11c compared to
181 $CX3CR1^{GFP/+}$ controls. Therefore, Axl regulates the acquisition of CD11c expression by microglia
182 (Figure 3F). Additionally, we found an increase in CD11c-expression with loss of CR3, though this is
183 likely due to a compensatory effect (26-28). Previously, we found Osteopontin (Spp1) RNA
184 expression in microglia to be downregulated with loss of Axl (5), and CD11c-expression has been
185 linked to Spp1-expression in various contexts (14, 29). Therefore, we assessed changes in Spp1
186 protein expression following loss of Axl signaling. We found the proportion and density of microglia
187 expressing Spp1 is significantly reduced compared to wildtype controls (Figure 3G – I). Taken
188 together, our results suggest CD11c+ microglia interact with apoptotic neurons, have increased
189 phagocytic activity, and are partially regulated by Axl signaling.
190
191 **Figure 3. CD11c+ microglia emerge from interactions with apoptotic cell bodies, mediated in**
192 **part by Axl signaling.** (A) Confocal image of P3 retinal flat mount (Arrowhead and magnified boxes
193 illustrate interactions) in NFL/GCL. CD11c-GFP+ microglia (green); cleaved caspase 3, CC3 (pink);
194 and RBPMS (blue). Scale bar, 50μm. (B) Percent CD11c-GFP+ microglia contacting apoptotic RGCs

195 (RBPMS+CC3+) at P3 out of total CD11c-GFP+ microglia within GCL. (n=5 animals). (C) Confocal
196 images of retinal flat mounts of P3 CD11c-GFP animals in GCL showing a range of microglial GFP
197 expression from none to high. Scale bar, 10µm. Dashed line demarcates distinction between CD11c-
198 GFP negative and positive. (D) Cell area immunostained for CD68 (*Top*) and C1q (*Bottom*) in CD11c-
199 GFP- and CD11c-GFP+ microglia (n=4 animals, 352 GFP- cells and 422 GFP+ cells). Mann-Whitney
200 test *Top* ***P* =.0011 and *Bottom* *****P* <.0001. (E) Scatter plot of CD68 area/cell compared to CD11c-
201 GFP area/cell at P3 in GCL. Pearson r= 0.4145 *****P* < .0001. (F) Flow cytometry analysis showing
202 the percent CD11c^{Hi} of total CD45+CD11b+ or CD45+CX3CR1-GFP+ microglia from retinas across
203 all genotypes. CX3CR1-GFP/+ (n=10), CX3CR1-KO (n=6), CR3 KO (n=6), MerTK KO (n=9), Axl KO
204 (n=8), and MerTK/Axl dKO (n=6), ≥ 2 litters collected for each genotype, ± SEM. One-way ANOVA
205 F(5, 39) = 34.64 *P*<.0001 and Tukey's multiple comparisons. *****P*<.0001, ****P*=.0003, ***P*=.0056,
206 **P*=.02, *NS,* not significant. (G) Max projected confocal image of P5 retinal flat mount from WT and
207 AXL KO, Spp1+ (green) and total microglia (IBA1+; red). Scale bar, 100µm. (H) Density of
208 Spp1+IBA1+ microglia in AXL WT and KO (n=5, n=4 animals) ± SEM. Unpaired t test **P* = .0139. (I)
209 Percent Spp1+IBA1+ of total IBA1+ microglia in AXL WT and KO (n=5, n=4 animals) ± SEM.
210 Unpaired t test ****P* <.001
211

212 CD11c+ microglia are not specifically required for phagocytic
213 clearance of apoptotic neurons

214 Next, we sought to determine whether CD11c+ microglia were specifically dedicated to the
215 phagocytic clearance of dying cells. We utilized two depletion strategies to target CD11c+ and non-
216 CD11c subsets (Figure 4A). First, to selectively ablate CD11c-GFP+ cells, we administered diphtheria
217 toxin (DT) to CD11c-DTR/GFP pups at P0, P2, and P4, and collected retinas at P5. Primate
218 diphtheria toxin receptor (DTR) expressed under the CD11c promoter allow for targeted ablation of
219 CD11c-GFP+ cells using DT (30). We confirmed that DT administration did not affect microglia

220 lacking expression of DTR as there was no change in total microglia density (C1q+/CX3CR1-GFP+)
221 in CX3CR1-GFP mice following the same DT administration paradigm (Supplemental Figure 3A, B).
222 DT administration to CD11c-DTR/GFP pups resulted in an ablation of ~75% of CD11c-GFP+
223 microglia, constituting a 25% reduction in the total microglia pool at P5 (Figures 4B – E). Conversely,
224 since we previously found that inhibition of CSF1R signaling eliminated homeostatic microglia while
225 enriching for CD11c+ microglia (6), for our second depletion paradigm we administered CSF1R
226 inhibitor pexidartinib (PLX 3397; (31)) to CX3CR1-GFP pups at P2 through P4, and collected at P5
227 (Figure 4A). As previously reported, we found the density of total C1q+ microglia was reduced by
228 approximately 50% in PLX3397 treated animals (Figures 4F, G). Confirming our previous findings that
229 CD11c-GFP+ microglia are less sensitive to CSF1R inhibition (5, 6), we found PLX3397 treatment
230 resulted in virtually no reduction in CD11c+ microglia density, with the proportion of CD11c-GFP+
231 microglia shifting from ~55% to ~85% (Supplementary Figure 3C – F). To determine whether
232 targeting these different microglia subsets had distinct effects on the clearance of apoptotic cells, we
233 analyzed the density of dying RGCs as assessed by persistence of cleaved caspase 3 labeled RGCs
234 (CC3+RBPMS+; Figure 4H). We found that DT-mediated depletion of CD11c-GFP+ microglia
235 significantly increased the density of apoptotic RGCs compared to both Vehicle and WT+DT controls
236 (Figure 4I). We showed the DT administration did not affect total RBPMS+ RGC number, confirming
237 DT did not induce RGC death (Supplemental Figure 3G, H). We found that PLX3397-mediated
238 microglia depletion also resulted in a significant persistence of apoptotic RGCs (Figures 4J). To
239 examine whether the buildup of apoptotic RGCs was proportional to microglia density regardless of
240 depletion strategy, we plotted CC3+RBPMS+ RGC density versus C1q+ microglia density from the
241 same animal. There was a strong negative correlation between total microglia density and dying RGC
242 density for either depletion strategy (Figure 4K). Overall, these findings suggest that CD11c-GFP+
243 microglia clear dying neurons, but are not selectively responsible or specialized to phagocytose
244 apoptotic cells.

245

246 **Figure 4. CD11c+ microglia are not solely responsible for phagocytic clearance of apoptotic**
247 **neurons.** (A) Depiction of two depletion strategies, Diphtheria toxin (DT) targeted ablation of CD11c-
248 DTR/GFP+ microglia (Top) and PLX3397 (PLX)-mediated depletion to target more homeostatic
249 microglia (Bottom). (B) Confocal images of CD11c-DTR/GFP+ microglia (green) in retinal flat mounts
250 at P5 of Vehicle and DT-treated CD11c-DTR/GFP mice. Scale bar, 50µm. (C) Density of CD11c-
251 DTR/GFP+ microglia in vehicle and DT-treated CD11c-DTR/GFP (n=6, n=7 animals) ± SEM.
252 Unpaired t test ****P <.0001. (D) Confocal images of C1q+ microglia (white) in immunostained retinal
253 flat mounts at P5 of vehicle and DT-treated CD11c-DTR/GFP mice. Scale bar, 50µm. (E) Densities of
254 C1q+ cells in retinas of vehicle and DT-treated CD11c-DTR/GFP mice (n=6, n=7 animals) ± SEM.
255 Mann Whitney test *P =.0140. (F) Max projected confocal images of C1q+ microglia in retinal flat
256 mounts at P5 of vehicle and PLX-treated Cx3CR1/GFP+ mice. C1q (white). Scale bar, 50µm. (G)
257 Density of C1q+ cells in retinas of naïve and PLX-treated CX3CR1-GFP (n=6, n=8) ± SEM. Unpaired
258 t test *P =.0239. (H) Max projected confocal images of apoptotic RGCs in retinal flat mounts at P5 of
259 all conditions/genotypes. CC3 (magenta); RBPMS (green). Scale bar, 50µm. (I) Density of
260 CC3+RBPMS+ cells in retinas from vehicle and DT-treated CD11c-DTR/GFP mice and DT-treated
261 wildtype mice (WT) (n=8, n=10, n=10 animals respectively) ± SEM. Ordinary one-way ANOVA **P
262 =.0018 and Tukey's multiple comparisons test: Veh vs DT **P =.006, WT+DT vs DT **P =.0043, *NS*,
263 not significant. (J) Density of CC3+RBPMS+ cells in naïve and PLX-treated CX3CR1-GFP/+ (n=8,
264 n=8 animals) ± SEM. Unpaired t test ****P <.0001 (K) Scatter plot of dying RGC density
265 (CC3+RBPMS+/mm^2) compared to microglial density (C1q+/mm^2) of same animal (n=4 CD11c +
266 vehicle, n=5 CD11c + DT, n=10 PLX animals). Pearson r= -0.6350 **P =.0035.

267

268 # Discussion

269 Single cell sequencing has revealed that microglia exist in diverse transcriptional states depending on
270 local environmental cues. Less is known, however, regarding how dynamic and reversible these
271 states are, the cues that produce specific states, and their relationship to cellular function. Here we
272 address this by examining the emergence and regulation of CD11c+ microglia in developing retina.
273 We first establish the recognition of apoptotic neurons as an important cue. CD11c+ microglia are
274 linked to developmental waves of neuronal apoptosis, are more phagocytic and interact with apoptotic
275 neurons, and expression of CD11c is modulated by signaling through the TAM receptor Axl, which
276 can recognize phosphatidylserine exposure by apoptotic neurons (32). Second, using lineage tracing
277 we provide evidence that microglia transition out of the CD11c+ state after the periods of neuronal
278 apoptosis end, demonstrating that this state is reversible. Finally, we used selective ablation
279 strategies to test whether CD11c+ microglia play a specialized role in apoptotic cell clearance and
280 found that they are not selectively responsible, and that all microglia can participate in the elimination
281 of apoptotic neurons. Altogether, this supports the notion that CD11c microglia in the retina arise from
282 exposure to dying cells.
283 CD11c+ microglia have been reported in association with Aβ plaques, in developing, aged, and
284 diseased white matter tracts of the brain, as well as the developing retina (8, 33). They have been
285 implicated in development and repair of myelinated tracts (8-10), but their abundance in the
286 developing retina, which lacks myelination, raises broader questions, including the environmental and
287 molecular context for their emergence during development. In adult retina, CD11c+ microglia density
288 is low, but following optic nerve crush, CD11c+ myeloid cells increase in number and play a
289 prominent role in the clearance of retinal ganglion cell and axonal debris (34), with evidence that
290 some CD11c+ cells are recruited into the retina from the myelinated optic nerve (35). The
291 transcriptional profile of CD11c+ microglia is overlapping with the transcriptome signatures described
292 for proliferative associate microglia (PAM) and axon tract associated microglia (ATM) in developing

293 brain, and related to gene signatures associated with aging and neurodegenerative disease (8, 11,
294 14, 36, 37), raising the possibility of related cues driving these microglial states.

295 CD11c+ microglia are driven by apoptosis.

296 We found previously ~50-60% of microglia within the developing postnatal retina express CD11c, and
297 that this proportion was significantly reduced in Bax KO retina (6), which lack neuronal apoptosis (38).
298 Here, we confirm that CD11c-GFP+ microglia density peaks postnatally in the retina and tracks with
299 developmental apoptosis. We found that the majority of CD11c-GFP+ microglia interact with apoptotic
300 cell bodies and have higher lysosomal content than their non-CD11c counterparts, consistent with
301 enhanced phagocytosis. CD11c+ microglia have been linked to phagocytosis in multiple contexts.
302 Within the developing brain, loss of “don’t-eat-me” signatures increases the number of CD11c+
303 microglia (39). While environmental cues driving this population in brain are unknown, consistent with
304 our data, CD11c+ microglia in white matter tracts of the developing brain have been shown to engulf
305 apoptotic oligodendrocytes and their precursors (4, 15). These data suggest microglial interactions
306 with apoptotic cells may promote acquisition of the CD11c+ state. Consistent with this, our lineage
307 analysis experiments found that CD11c-active microglia were more ameboid, had more phagocytic
308 cups, and concentrated to layers undergoing developmental apoptosis whereas CD11c-lineage
309 microglia had a branched morphology, less phagocytic cups, and distributed normally across all
310 retinal layers. Despite this, we found that CD11c-GFP+ microglia were not any more efficient at the
311 clearance of apoptotic neurons than their CD11c-negative counterparts. We found that the clearance
312 of apoptotic neurons was directly proportional to the total number of microglia available, suggesting
313 phagocytic clearance is not augmented in CD11c+ microglia.

314 CD11c acquisition is regulated by Axl signaling.

315 Our data and others show that the recognition of eat-me signatures is important for the acquisition of
316 CD11c+ signature (5, 6, 9, 14, 29, 40). Conversely, “don’t eat-me” signature, Sirpα and CD47, were
317 shown to constrain CD11c-expression through repression of eat-me signatures (39, 41). We found

318 that early postnatal retina in Axl KO have a significant reduction in CD11c+ microglia, matching levels
319 of CD11c+ microglia in Bax KO (6). We also found that microglial expression of Spp1 was reduced by
320 Axl KO, consistent with other studies showing Spp1 expression by CD11c+ microglia (5, 14). In fact,
321 CD11c+ microglia were reported to be the sole producer of Spp1 in the brain (14), and axon tract
322 associated/CD11c+ microglia were shown to co-express Spp1 and were found to maintain structural
323 integrity at cortical boundaries during fetal development (42). Taken together, our data implicate Axl
324 in regulating the CD11c+ microglia state.
325 A previous study also implicated TAM receptors in the regulation of CD11c, with blockage of
326 apoptotic neuron uptake through the inhibition of pan-Tam receptors and αVβ3 resulting in a marked
327 reduction of CD11c-expression by microglia (43). However, we have previously shown that Axl is not
328 required for the uptake and clearance of apoptotic neurons (5), suggesting that other Axl-mediated
329 mechanisms may be involved. Interestingly, we also observed a marked increase in the proportion of
330 microglia expression CD11c in CR3 KOs, suggesting a potential compensation by CD11c (CR4) for
331 the loss of complement recognition by CD11b (CR3). CR3 is broadly expressed by microglia and is
332 involved in the recognition of stressed or dying neurons in a variety of contexts, including the
333 elimination of stressed RGCs embryonically and dying RGCs postnatally (5, 44). The observed
334 increase in CD11c-expression with loss of CR3 expression may be attributed to compensatory
335 upregulation, as both CR3 and CR4 are capable of recognizing deposition of iC3b, albeit CR4 is less
336 readily positioned to bind iC3b under normal conditions (26, 27). Altogether, CD11c expression
337 appears directly tied to the balance of eat-me cues versus don't eat me cues, with a reduction of eat-
338 me signaling through Axl translating into a reduction of CD11c+ microglia, and conversely, a
339 reduction of don't eat-me signals (like Sirpα and CD47) translating into an increase in CD11c+
340 microglia (39, 41).

341 **CD11c+ microglia are a transient and dynamically regulated state.**

342 With the proportion of CD11c + microglia in the retina declining as development progresses into
343 adulthood, we asked whether CD11c+ microglia reintegrated back into the “homeostatic” pool of
344 microglia. In brain, CD11c+ microglia are most abundant in cortical white matter tracts between
345 postnatal days 3 through 8, with a sharp decline into adulthood (9, 10). Additionally, *in vitro*
346 experiments show Cd11c-negative microglia, when cultured with apoptotic neurons, acquire CD11c-
347 expression (14). These findings and fate-mapping experiments suggest CD11c+ microglia have the
348 same origin as other brain microglia and do not arise from peripheral immune populations (10, 39).
349 Here, we found that the proportion of CD11c-GFP+ microglia density dramatically shifts over time.
350 Using a genetic lineage-tracing strategy, we find evidence that CD11c+ microglia reintegrate into the
351 homeostatic pool of microglia within the retina, since from P5 to P30 the loss of CD11c-active
352 microglia was proportional to the increase in CD11c-lineage microglia while the CD11c-negative
353 microglia remain stable. To date, there have been conflicting data on whether CD11c+ microglia
354 represent a stable subset that emerges in development and is maintained through adulthood (8, 9,
355 11), or a state achieved through recognition of molecular cue(s) (5, 6, 14). Altogether, our data
356 suggest CD11c expression is transiently expressed in response to exposure to apoptotic neurons,
357 and microglia shift back into a CD11c- state rather than being maintained as a stable subset.
358

359 Materials

360 Animal husbandry and procedures

361 Animals were treated within the University of Utah Institutional Animal Care and Use Committee
362 (IACUC) guidelines and approval. Mice were housed in an AAALAC accredited animal facility with
363 12h light/12h dark cycles and ad libitum access to food and water. Both sexes were used for all
364 experiments. PLX3397 (AdooQ BioScience,A15520) was dissolved in corn oil and 10% DMSO and
365 administered to postnatal pups by intraperitoneal injection on P2-P4 at 0.125 mg/g body weight.

366 Diphtheria Toxin (List Labs, #150) was dissolved in PBS and administered to postnatal pups by
367 intraperitoneal injection at P0, P2, and P4 at 5ng/g of body weight.

368 Mouse strains

369 The B6.129P2 (Cg)-*Cx3cr1*^{tm1Litt}/J mice (22) were a gift from Richard Lang with permission from
370 Steffen Jung. B6.FVB-*1700016L21Rik*$^{Tg(Itgax\text{-}DTR/EGFP)57Lan}$/J (JAX 004509), C57BL/6J-Tg(Itgax-cre,-
371 EGFP)4097Ach/J (JAX 007567), B6.Cg-*Gt(Rosa)26Sor*$^{tm14(CAG\text{-}tdTomato)Hze}$/J (JAX 007914), and
372 B6.129S4-Itgam^{tm1Myd}/J (JAX 003991) were purchased from Jackson laboratories. The B6.129-
373 Mertk^{tm1Grl}/J and B6.129-Axl^{tm1Grl}/J strains (25) were a gift from Dr. Greg Lemke.

374 Tissue processing

375 Mice were decapitated following isoflurane asphyxiation, and whole heads were fixed in 4% PFA for
376 45 minutes to an hour. Heads were washed 3 times for 15 minutes in PBS and underwent 12–16-
377 hour consecutive treatments with 15% and 30% sucrose in PBS at 4°C. Heads were then embedded
378 in OCT compound (Tissue-Tek), stored at 80°C, and sectioned at 16μm or 30μm thickness. For
379 retinal flat mounts, eyes were removed from the head and retinas were carefully dissected from the
380 rest of the eye in ice cold 0.1M PBS, then washed in PBS for 10mins, and fixed in 4% PFA for 40mins
381 at room temperature. For flow cytometry/FACS experiments, retinas were dissected RNAse-free
382 conditions.

383 Immunohistochemistry

384 Frozen sections were placed in ice-cold PBS for 10min, post-fixed for 10min in 4% PFA, washed in
385 ice-cold PBS 3 times for 5min each, and then blocked for 1 hr at room temperature (0.2% triton-X,
386 10% BSA, 10% normal donkey serum in 0.01M PBS). Sections were incubated in primary antibody
387 overnight at 4ºC (0.2% triton-X, 5% BSA in 0.01M PBS). The following day, sections were washed 3
388 times with PBS for 5min each and incubated in secondary antibodies (5% BSA in 0.01M PBS) with
389 Hoechst 33342 (1:5000, Thermo Fischer Scientific H3570) for 2 hrs at room temperature, washed,

390 and mounted with Fluoroshield mounting medium with DAPI (Millipore Sigma, F6057). Flat mount
391 immunostaining followed the same protocol except for primary antibody incubation, with flat mounts
392 incubated in primary antibodies at 4ºC for 2 days. Antibodies used include Goat polyclonal anti-GFP
393 (1:2000, Abcam ab5450, RRID: AB_304897), Rabbit monoclonal anti-C1q (1:1500, Abcam
394 an182451, RRID: AB_2732849), Rabbit polyclonal anti-IBA1 (1:1000, Wako 019-19741, RRID:
395 AB_839504), Rabbit monoclonal anti-CC3 (1:500, BD Biosciences 559565, RRID: AB_397274),
396 Guinea pig polyclonal anti-RBPMS (1:750, Millipore Sigma ABN1376, RRID: AB_2687403), Rat
397 monoclonal anti-CD68 (1:250, Bio-Rad MCA1957, RRID: AB_322219), and Goat polyclonal anti-
398 Osteopontin (1:100, Thermo Fischer PA5-34579, RRID: AB_2551931). Secondary antibodies were
399 produced in donkey against goat, mouse, rabbit, guinea pig, and rat IgG, and conjugated to
400 AlexaFluor -488, -555, or -647 (Thermo Fisher Scientific).

401 Confocal microscopy

402 Confocal images were acquired on an inverted Nikon A1R Confocal Microscope, with images
403 acquired at 20X objective and 3X digital zoom and 10% overlap multi-point stitching. Z plane stacks
404 were at 0.8μm steps, with ~13μm thickness to capture the NFL/GCL at 0.2mm pixel resolution. Flat
405 mount retina images represent maximal-intensity projections of inner retina, primarily targeting GCL
406 (NFL/GCL) from the central retina to the periphery, and acquisition settings were consistent across
407 ages and genotypes.

408 Fluorescence-activated cell sorting (FACS) and flow cytometry

409 2 retinas from an individual animal were pooled for each sample for Flow cytometry and FACS.
410 Freshly dissected pure retinas were dissociated in PBS, 50 mM HEPES, 0.05 mg/ml DNase I (Sigma
411 D4513), 0.025 mg/ml Liberase (Sigma 5401119001) for 35 min with intermediate trituration. Cells
412 were passed through a 70 μm nylon cell strainer, washed with staining buffer (1X PBS, 2% BSA,
413 0.1% sodium azide, 0.05% EDTA), and red blood cells were lysed (eBioscience 00-4333-57). Cell
414 counts were determined using a cell counter (Invitrogen Countess) and Fc block (BD Biosciences

415 553142) was added at 2 mL per 10^6 cells. Antibodies used: BV421 Rat monoclonal anti-CD45 (BD
416 Bioscience 563890, RRID: AB_2651151), AF 700 Rat monoclonal anti-CD11b (BD Bioscience
417 557960, RRID: AB_396960), PE-Cy7 Rat monoclonal anti-Ly6C (BD Bioscience 560593, RRID:
418 AB_1727557), APC Hamster monoclonal anti-CD11c (BD Bioscience Pharmingen 561119, RRID:
419 AB_10562405), and APC Rat monoclonal CD206 (Thermo Fisher Scientific 141708, RRID:
420 AB_10896057) were applied for 30 min on ice. Cells were washed, pelleted, and resuspended in 500
421 µL staining buffer. FACS was performed using a BD FACS Aria cell sorter at the University of Utah
422 Flow Cytometry Core. Forward and side scatter were used to eliminate debris and both the width and
423 area of the forward and side scatter was used to discriminate singlets. ~1 million singlet events were
424 recorded for analysis, and gates for flow analysis were determined using FMO control. Analysis was
425 conducted using FlowJo software (Flowjo, LLC, Ashland, Oregon).

426 CD11c-lineage bulk-seq

427 Bulk RNA-sequencing was performed on FACs sorted cells from CD11c-Cre-gfp;Rosa-TDTom
428 animals at P5. One sample each of Cd11c lineage cells (GFP-TdTom+, 5441 cells) and Cd11c active
429 cells (GFP+TdTom+, 4041 cells) were sorted from 8 retinas (4 female and 4 male). Total RNA was
430 prepared with the RNeasy Plus Kit (Qiagen 74034) and RNA Clean and Concentrator kit (Zymo
431 R1013) and hybridized with NEBNext rRNA Depletion Kit v2 (NEB E7400) to substantially diminish
432 rRNA from the samples. Stranded RNA sequencing libraries were prepared as described using the
433 NEBNext Ultra II Directional RNA Library Prep Kit for Illumina (NEB E7760L). Purified libraries were
434 qualified on an Agilent Technologies 4150 TapeStation using a D1000 ScreenTape assay (5067-5582
435 and 5067-5583). The molarity of adapter-modified molecules was defined by quantitative PCR using
436 the Kapa Biosystems Kapa Library Quant Kit (KK4824). Individual libraries were normalized to 5 nM
437 in preparation for Illumina sequence analysis. Libraries were sequenced on an Illumina NovaSeq
438 6000 S4 with reagent kit v1.5 to produce 150x150 bp paired-end sequences to a depth of greater
439 than 50 million paired reads. Illumina adapters were trimmed from reads with cutadapt v3.5, trimming

440 after 6 matching bases and discarding trimmed reads shorter than 20 bases. Trimmed reads were
441 aligned with STAR v2.7.9a in two pass mode to indexed genome GRCm39, created with splice
442 junctions from Ensembl release 104 and a maximum overhang of 124 bases, to generate a BAM
443 alignment file sorted by coordinates. Uniquely aligned fragment counts were assigned to Ensembl
444 104 transcripts from the alignment files with featureCounts v1.6.3.edgeR v4.0.16 was used to
445 calculate log fold changes and log CPM from read counts with the exactTest function. Raw and
446 processed data files are available at the Gene Expression Omnibnus under GEO accession number
447 GSE269549.;

448 **Image analysis**

449 All counts were blinded and manually performed using Nikon Elements software (Melville, NY). For
450 double positive CC3+RBPMS+ or single RBPMS+ counts of retinal flat mounts, two ROIs of roughly
451 0.4 mm^2 of central and periphery of dorsal retina were analyzed. Images were maximal-intensity
452 projected and roughly 13µm thick, spanning the NFL to the GCL. For quantification of CD11c-GTFP+
453 microglia in retinal flat mounts, the entire retina, ranging from 1.5 to 8 mm^2, was analyzed across all
454 retinal depths, ranging from 25 to 55µm. Microglial proportion was determined as CD11c-GFP+/total
455 microglia (C1q+). CD11c-GFP+ localization analysis was performed on entire cross sections of 3
456 retinas. For 3D reconstructions of microglia-apoptotic body interactions, IMARIS software (Bit-plane)
457 was used. In brief, high resolution confocal images (20X objective, 8X digital zoom) through Z
458 (0.16µm steps) were uploaded into IMARIS to create 3D renderings. For CD68 and C1q area
459 analysis, P3 retinal flat mount imaging and analysis spanned ~13µm spanning the NFL to GCL only
460 for the dorsal quadrant of the right eye of each animal analyzed. The lysosomal content (CD68 area)
461 was analyzed against total microglia area (union of C1q and CD68 channels), with quantification of
462 CD68/C1q+CD68 in CD11c-GFP+ versus CD11c-GFP- microglia. For phagocytic cup analysis, a
463 “phagocytic cup” was determined based upon a cup-shaped invagination of the plasma membrane
464 formed around cellular debris or dying/dead cells located at the tip of microglial processes. Microglia

465 phagocytic cups were counted in P5 retinal flat mounts stained with CD68 in CD11c-Cre$^{GFP/+}$;
466 Rosa$^{tdTomato/+}$, focusing on CD11c-active (GFP+tdTomato+) and CD11c-lineage (GFP-tdTomato+)
467 microglia.

468 ## Statistical methods

469 All image and flow data were analyzed using Prism 10 software (GraphPad, La Jolla, CA). We first
470 tested for normality using four tests: Anderson-Darling, D'Agostino & Pearson, Shapiro-Wilk, and
471 Kolmogorov-Smirnov test. Failure of any one test resulted in non-parametric tests, Mann-Whitney for
472 pair-wise comparisons and Kruskal-Wallis for comparisons of more than three samples. We tested for
473 heteroscedasticity using an F-test for pairwise comparisons and Brown-Forsythe test for comparisons
474 of three or more. If not significantly different, we either ran a two-tailed T test, Ordinary one-way
475 ANOVA with posthoc Tukey's multiple comparison test, or Ordinary two-way ANOVA with Sidak's
476 multiple comparison test. If standard deviations were significantly different between groups, we ran a
477 Welch's ANOVA with posthoc Dunnett's T3 multiple comparison's test. For all data that is presented
478 as the mean, error bars indicate the standard error of the mean, SEM. We used a 95% confidence
479 interval and a P value of $< .05$ was set for rejecting the null hypothesis.
480

481 # Supporting information

482 **Supplementary Figure S1. CD11c-GFP correlates with microglia surface expression of CD11c.**
483 **Related to Figure 1.** (A) (left) Gating strategy for FACS of CD45+CD11b+ microglia and (right)
484 CD11c-GFP expression with CD11c-antibody (APC). (bottom) Histogram of CD11c+ and CD11c-
485 populations along CD11c-GFP+ signal. Left and bottom back colored based on gating on the right.
486 **Supplementary Figure S2. Flow cytometry analysis of CD11c^{Hi} microglia with loss of candidate**
487 **receptors. Related to Figure 3.** (A – F) Representative flow plots illustrating the proportion of
488 CD45+GFP+ or CD45+CX3CR1-GFP+ microglia that are CD11c^{Hi}. ≥ 2 litters collected for each

489 genotype, with (A) CX3CXR1-GFP/+ n=10 (B) CX3CR1 KO n=6, (C) CR3 KO n=6, (D) MerTK KO
490 n=9, (E) Axl KO n=8, and (F) MerTK/Axl dKO n=6 animals.

491 **Supplementary Figure S3. Diphtheria toxin administration does not affect microglia without**
492 **primate DTR expression, PLX administration enriches for CD11c-GFP+ microglia. Related to**
493 **Figure 4.**

494 (A) Confocal images of microglia (C1q+) in retinal flat mounts at P5 of Vehicle and DT-treated
495 CX3CR1-GFP/+ mice. C1q+ (white). Scale bar, 50μm. (B) Density of C1q+ microglia in vehicle and
496 DT-treated CX3CR1-GFP/+ mice at P5 (n=2 animals) ± SEM. Unpaired t test *NS,* not significant. (C)
497 Confocal retinal flat mount images from naïve and PLX treated CD11c-DTR/GFP+ mice at P5.
498 CD11c-DTR/GFP microglia (GFP+IBA1+) and total microglia (IBA1+, red) Scale bar, 50μm. (D – F)
499 Densities of naïve and PLX treated CD11c-DTR/GFP+ mice, with (D) total microglia density (IBA1+;
500 n=3, n=3 animals), (E) CD11c-DTR/GFP+ microglia density (IBA1+CD11c-DTR/GFP+; n=3, n=3
501 animals), and (F) proportion of microglia (IBA1+) expressing CD11c-DTR/GFP (n=3, n=3 animals) ±
502 SEM. Unpaired t test ***P = .0004, *P = .0340, *NS*, not significant. (G) Confocal images of RGCs
503 (RBPMS+) in retinal flat mounts at P5 of vehicle and DT treated CD11c-DTRG/GFP+. RBPMS
504 (white). Scale bar, 50μm. (H) Densities of vehicle and DT-treated CD11c-DTR/GFP RGCs in (Left)
505 central region and (Right) peripheral region of dorsal leaf (vehicle n=4, DT n=8 animals) ± SEM.
506 Unpaired t test *NS,* not significant, Scale bars, 50μm.

507

508 # Acknowledgments

509 Cartoons were created with BioRender. We thank the University of Utah Office of Comparative
510 Medicine for animal husbandry. Research reported in the publication utilized the University of Utah
511 Flow Cytometry Core at Huntsman Cancer Institute at the University of Utah, which is supported by
512 the Office of the Director of the NIH and NCI. Research reported in this publication utilized the High-
513 Throughput Genomics and Bioinformatic Analysis Shared Resource at the Huntsman Cancer Institute

at the University of Utah. The support and resources from the Center for High Performance Computing at the University of Utah are gratefully acknowledged. This content is solely the responsibility of the authors and does not necessarily represent the official views of the NIH.

Funding

This work was supported by the National Eye Institute and the National Institutes of Neurological Disorders and Stroke of the National Institutes of Health, under awards R01EY030307 and R21EY034753 (MLV), and T32EY024234, T32NS115664, and F31EY035163 (NG). Research reported in the publication utilized the University of Utah Flow Cytometry Core at Huntsman Cancer Institute and the Center for High Performance Computing at the University of Utah, under award numbers P30CA042014, S10OD026959, and 5P30CA042014-24 from the Office of the Director of National Institutes of Health and National Cancer Institute.

Author contributions

Conceptualization: Nathaniel Ghena, Sarah R Anderson, Monica L Vetter

Formal analysis: Nathaniel Ghena, Sarah R Anderson, Jacqueline M Roberts, Emmalyn Irvin, Joon Schwakopf, Alejandra Bosco

Funding acquisition: Nathaniel Ghena, Monica L Vetter

Investigation: Nathaniel Ghena, Sarah R Anderson, Jacqueline M Roberts, Monica L Vetter

Methodology: Nathaniel Ghena, Sarah R Anderson, Jacqueline M Roberts, Emmalyn Irvin, Joon Schwakopf, Alejandra Bosco, Monica L Vetter

535 **Resources:** Nathaniel Ghena, Sarah R Anderson, Joon Schwakopf, Emmalyn Irvin, Monica L
536 Vetter
537 **Visualization:** Nathaniel Ghena, Sarah R Anderson, Jacqueline M Roberts
538 **Writing – original draft:** Nathaniel Ghena, Sarah R Anderson, Monica L Vetter
539 **Writing – review & editing:** Nathaniel Ghena, Sarah R Anderson, Jacqueline M Roberts,
540 Emmalyn Irvin, Joon Schwakopf, Alejandra Bosco, Monica L Vetter
541

542 # References

543 1. Paolicelli RC, Sierra A, Stevens B, Tremblay ME, Aguzzi A, Ajami B, et al. Microglia states and
544 nomenclature: A field at its crossroads. Neuron. 2022;110(21):3458-83.
545 10.1016/j.neuron.2022.10.020
546 2. Prinz M, Masuda T, Wheeler MA, Quintana FJ. Microglia and Central Nervous System-
547 Associated Macrophages-From Origin to Disease Modulation. Annu Rev Immunol. 2021;39:251-77.
548 10.1146/annurev-immunol-093019-110159
549 3. Hammond TR, Dufort C, Dissing-Olesen L, Giera S, Young A, Wysoker A, et al. Single-Cell
550 RNA Sequencing of Microglia throughout the Mouse Lifespan and in the Injured Brain Reveals
551 Complex Cell-State Changes. Immunity. 2019;50(1):253-71 e6. 10.1016/j.immuni.2018.11.004
552 4. Li Q, Cheng Z, Zhou L, Darmanis S, Neff NF, Okamoto J, et al. Developmental Heterogeneity
553 of Microglia and Brain Myeloid Cells Revealed by Deep Single-Cell RNA Sequencing. Neuron.
554 2019;101(2):207-23 e10. 10.1016/j.neuron.2018.12.006
555 5. Anderson SR, Roberts JM, Ghena N, Irvin EA, Schwakopf J, Cooperstein IB, et al. Neuronal
556 apoptosis drives remodeling states of microglia and shifts in survival pathway dependence. Elife.
557 2022;11 10.7554/eLife.76564

558 6. Anderson SR, Roberts JM, Zhang J, Steele MR, Romero CO, Bosco A, et al. Developmental
559 Apoptosis Promotes a Disease-Related Gene Signature and Independence from CSF1R Signaling in
560 Retinal Microglia. Cell Rep. 2019;27(7):2002-13 e5. 10.1016/j.celrep.2019.04.062
561 7. Pitts KM, Margeta MA. Myeloid masquerade: Microglial transcriptional signatures in retinal
562 development and disease. Front Cell Neurosci. 2023;17:1106547. 10.3389/fncel.2023.1106547
563 8. Benmamar-Badel A, Owens T, Wlodarczyk A. Protective Microglial Subset in Development,
564 Aging, and Disease: Lessons From Transcriptomic Studies. Front Immunol. 2020;11:430.
565 10.3389/fimmu.2020.00430
566 9. Wlodarczyk A, Holtman IR, Krueger M, Yogev N, Bruttger J, Khorooshi R, et al. A novel
567 microglial subset plays a key role in myelinogenesis in developing brain. EMBO J. 2017;36(22):3292-
568 308. 10.15252/embj.201696056
569 10. Hagemeyer N, Hanft KM, Akriditou MA, Unger N, Park ES, Stanley ER, et al. Microglia
570 contribute to normal myelinogenesis and to oligodendrocyte progenitor maintenance during
571 adulthood. Acta Neuropathol. 2017;134(3):441-58. 10.1007/s00401-017-1747-1
572 11. Nomaki K, Fujikawa R, Masuda T, Tsuda M. Spatiotemporal dynamics of the CD11c(+)
573 microglial population in the mouse brain and spinal cord from developmental to adult stages. Mol
574 Brain. 2024;17(1):24. 10.1186/s13041-024-01098-2
575 12. Kamphuis W, Kooijman L, Schetters S, Orre M, Hol EM. Transcriptional profiling of CD11c-
576 positive microglia accumulating around amyloid plaques in a mouse model for Alzheimer's disease.
577 Biochim Biophys Acta. 2016;1862(10):1847-60. 10.1016/j.bbadis.2016.07.007
578 13. Keren-Shaul H, Spinrad A, Weiner A, Matcovitch-Natan O, Dvir-Szternfeld R, Ulland TK, et al.
579 A Unique Microglia Type Associated with Restricting Development of Alzheimer's Disease. Cell.
580 2017;169(7):1276-90 e17. 10.1016/j.cell.2017.05.018

581 14. Shen X, Qiu Y, Wight AE, Kim HJ, Cantor H. Definition of a mouse microglial subset that
582 regulates neuronal development and proinflammatory responses in the brain. Proc Natl Acad Sci U S
583 A. 2022;119(8) 10.1073/pnas.2116241119
584 15. Nemes-Baran AD, White DR, DeSilva TM. Fractalkine-Dependent Microglial Pruning of Viable
585 Oligodendrocyte Progenitor Cells Regulates Myelination. Cell Rep. 2020;32(7):108047.
586 10.1016/j.celrep.2020.108047
587 16. Jung S, Unutmaz D, Wong P, Sano G-I, De los Santos K, Sparwasser T, et al. In Vivo
588 Depletion of CD11c+ CD8+ Dendritic Cells Abrogates Priming of T Cells by Exogenous Cell-
589 Associated Antigens. Immunity. 2002;17(2):211-20.
590 17. Young RW. Cell Death During Differentiation of the Retina in the Mouse. Journal of
591 Comparative Neurology. 1984;229:362-73.
592 18. Santos AM, Calvente R, Tassi M, Carrasco MC, Martin-Oliva D, Marin-Teva JL, et al.
593 Embryonic and postnatal development of microglial cells in the mouse retina. J Comp Neurol.
594 2008;506(2):224-39. 10.1002/cne.21538
595 19. Stranges PB, Watson J, Cooper CJ, Choisy-Rossi CM, Stonebraker AC, Beighton RA, et al.
596 Elimination of antigen-presenting cells and autoreactive T cells by Fas contributes to prevention of
597 autoimmunity. Immunity. 2007;26(5):629-41. 10.1016/j.immuni.2007.03.016
598 20. Madisen L, Zwingman TA, Sunkin SM, Oh SW, Zariwala HA, Gu H, et al. A robust and high-
599 throughput Cre reporting and characterization system for the whole mouse brain. Nat Neurosci.
600 2010;13(1):133-40. 10.1038/nn.2467
601 21. Krasemann S, Madore C, Cialic R, Baufeld C, Calcagno N, El Fatimy R, et al. The TREM2-
602 APOE Pathway Drives the Transcriptional Phenotype of Dysfunctional Microglia in
603 Neurodegenerative Diseases. Immunity. 2017;47(3):566-81 e9. 10.1016/j.immuni.2017.08.008

604 22. Jung S, Aliberti J, Graemmel P, Sunshine MJ, Kreutzberg GW, Sher A, et al. Analysis of
605 fractalkine receptor CX(3)CR1 function by targeted deletion and green fluorescent protein reporter
606 gene insertion. Mol Cell Biol. 2000;20(11):4106 - 1414. doi: 10.1128/MCB.20.11.4106-4114.2000
607 23. Coxon A, Rieu P, Barkalow FJ, Askari S, Sharpe AH, von Andrian UH, et al. A Novel Role for
608 the beta-2 Integrin CD11b/CD18 in Neutrophil Apoptosis: A Homeostatic Mechanism in Inflammation.
609 Immunity. 1996;5:653-66.
610 24. Fourgeaud L, Traves PG, Tufail Y, Leal-Bailey H, Lew ED, Burrola PG, et al. TAM receptors
611 regulate multiple features of microglial physiology. Nature. 2016;532(7598):240-4.
612 10.1038/nature17630
613 25. Lu Q, Gore M, Zhang Q, Camenisch T, Boast S, Casagranda F, et al. Tyro-3 family receptors
614 are essential regulators of mammalian spermatogenesis. Nature. 1999;398(6729):723 - 8. doi:
615 10.1038/19554
616 26. Sandor N, Lukacsi S, Ungai-Salanki R, Orgovan N, Szabo B, Horvath R, et al. CD11c/CD18
617 Dominates Adhesion of Human Monocytes, Macrophages and Dendritic Cells over CD11b/CD18.
618 PLoS One. 2016;11(9):e0163120. 10.1371/journal.pone.0163120
619 27. Ross GD, Reed W, Dalzell JG, Becker SE, Hogg N. Macrophage cytoskeleton association with
620 CR3 and CR4 regulates receptor mobility and phagocytosis of iC3b-opson ized erythrocytes. Journal
621 of Leukocyte Biology. 1992;51:109-17.
622 28. Probst HC, Tschannen K, Odermatt B, Schwendener R, Zinkernagel RM, Van Den Broek M.
623 Histological analysis of CD11c-DTR/GFP mice after in vivo depletion of dendritic cells. Clin Exp
624 Immunol. 2005;141(3):398-404. 10.1111/j.1365-2249.2005.02868.x
625 29. Qiu Y, Shen X, Ravid O, Atrakchi D, Rand D, Wight AE, et al. Definition of the contribution of
626 an Osteopontin-producing CD11c(+) microglial subset to Alzheimer's disease. Proc Natl Acad Sci U S
627 A. 2023;120(6):e2218915120. 10.1073/pnas.2218915120

628 30. Pappenheimer AM, Harper AA, Moynihan M, Brockes JP. Diphtheria Toxin and Related
629 Proteins: Effect of Route of Injection on Toxicity and the Determination of Cytotoxicity for Various
630 Cultured Cells. The Journal of Infectious Disease. 1982;145:94-102.
631 31. Elmore MR, Najafi AR, Koike MA, Dagher NN, Spangenberg EE, Rice RA, et al. Colony-
632 stimulating factor 1 receptor signaling is necessary for microglia viability, unmasking a microglia
633 progenitor cell in the adult brain. Neuron. 2014;82(2):380-97. 10.1016/j.neuron.2014.02.040
634 32. Lemke G. Phosphatidylserine Is the Signal for TAM Receptors and Their Ligands. Trends
635 Biochem Sci. 2017;42(9):738-48. 10.1016/j.tibs.2017.06.004
636 33. Anderson SR, Vetter ML. Developmental roles of microglia: A window into mechanisms of
637 disease. Dev Dyn. 2019;248(1):98-117. 10.1002/dvdy.1
638 34. Lehmann U, Heuss ND, McPherson SW, Roehrich H, Gregerson DS. Dendritic cells are early
639 responders to retinal injury. Neurobiol Dis. 2010;40(1):177-84. 10.1016/j.nbd.2010.05.022
640 35. Heuss ND, Pierson MJ, Roehrich H, McPherson SW, Gram AL, Li L, et al. Optic nerve as a
641 source of activated retinal microglia post-injury. Acta Neuropathol Commun. 2018;6(1):66.
642 10.1186/s40478-018-0571-8
643 36. Holtman IR, Raj DD, Miller JA, Schaafsma W, Yin Z, Brouwer N, et al. Induction of a common
644 microglia gene expression signature by aging and neurodegenerative conditions: a co-expression
645 meta-analysis. Acta Neuropathol Commun. 2015;3:31. 10.1186/s40478-015-0203-5
646 37. Holtman IR, Skola D, Glass CK. Transcriptional control of microglia phenotypes in health and
647 disease. J Clin Invest. 2017;127(9):3220-9. 10.1172/JCI90604
648 38. Pequignot MO, Provost AC, Salle S, Taupin P, Sainton KM, Marchant D, et al. Major role of
649 BAX in apoptosis during retinal development and in establishment of a functional postnatal retina.
650 Dev Dyn. 2003;228(2):231-8. 10.1002/dvdy.10376

651 39. Sato-Hashimoto M, Nozu T, Toriba R, Horikoshi A, Akaike M, Kawamoto K, et al. Microglial
652 SIRPalpha regulates the emergence of CD11c(+) microglia and demyelination damage in white
653 matter. Elife. 2019;8 10.7554/eLife.42025
654 40. Kohno K, Shiraska R, Yoshihara K, Mikuriya S, Tanaka K, Takanami K, et al. A spinal
655 microglia population invovled in remitting and relapsing neuropathic pain. Science. 2022;376:86-90.
656 DOI:10.1126/science.abf6805
657 41. Wu J, Wu H, An J, Ballantyne CM, Cyster JG. Critical role of integrin CD11c in splenic
658 dendritic cell capture of missing-self CD47 cells to induce adaptive immunity. Proc Natl Acad Sci U S
659 A. 2018;115(26):6786-91. 10.1073/pnas.1805542115
660 42. Lawrence AR, Canzi A, Bridlance C, Olivie N, Lansonneur C, Catale C, et al. Microglia
661 maintain structural integrity during fetal brain morphogenesis. Cell. 2024;187(4):962-80 e19.
662 10.1016/j.cell.2024.01.012
663 43. Zagorska A, Traves PG, Lew ED, Dransfield I, Lemke G. Diversification of TAM receptor
664 tyrosine kinase function. Nat Immunol. 2014;15(10):920-8. 10.1038/ni.2986
665 44. Anderson SR, Zhang J, Steele MR, Romero CO, Kautzman AG, Schafer DP, et al.
666 Complement Targets Newborn Retinal Ganglion Cells for Phagocytic Elimination by Microglia. J
667 Neurosci. 2019;39(11):2025-40. 10.1523/JNEUROSCI.1854-18.2018
668

Figure 1.

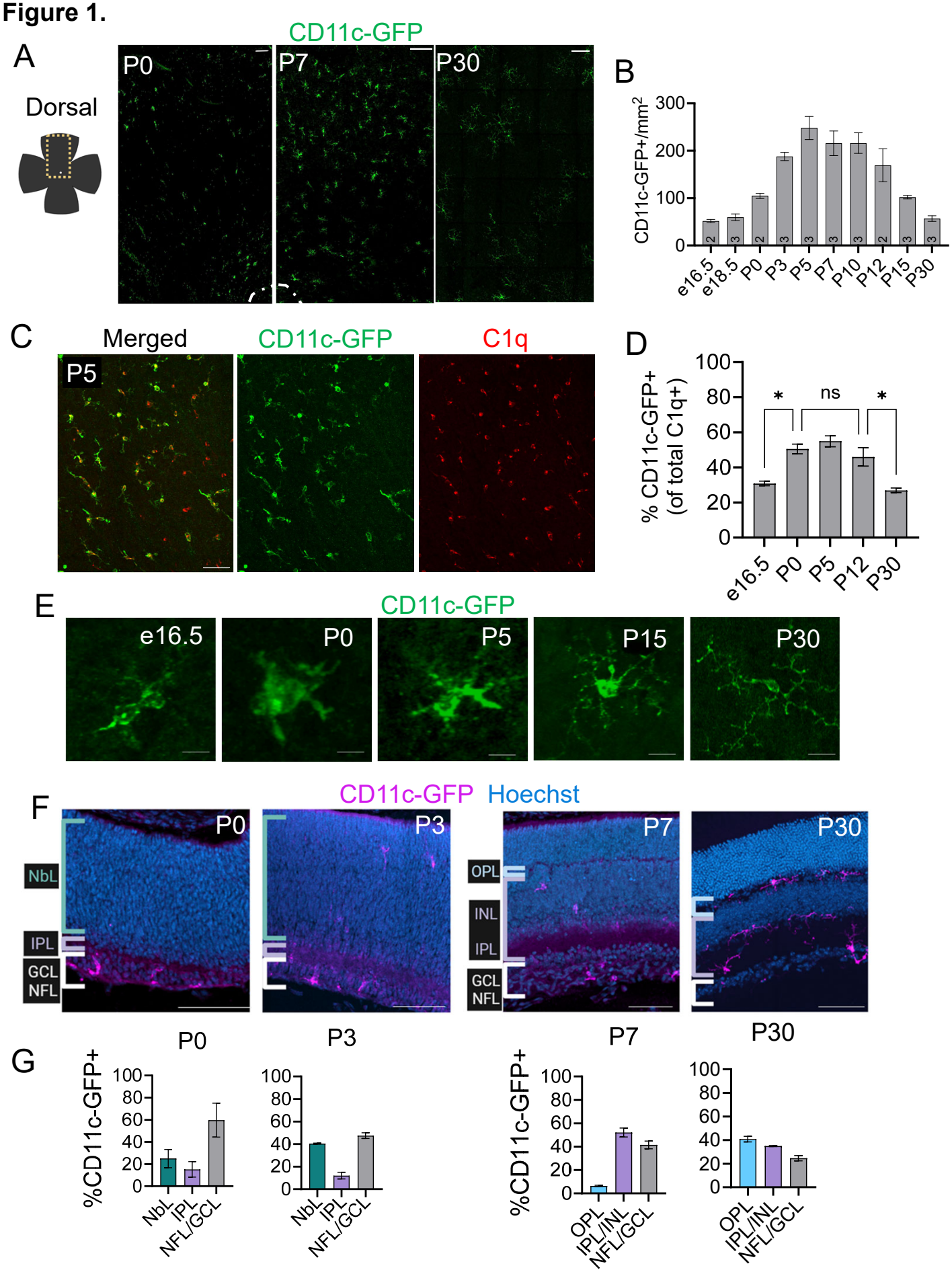
A
Dorsal
CD11c-GFP
P0
P7
P30
B
CD11c-GFP+/mm²
300
200
100
0
2
3
2
3
3
3
3
2
3
3
e16.5
e18.5
P0
P3
P5
P7
P10
P12
P15
P30
C
Merged
CD11c-GFP
C1q
P5
D
% CD11c-GFP+
(of total C1q+)
100
80
60
40
20
0
*
ns
*
e16.5
P0
P5
P12
P30
E
CD11c-GFP
e16.5
P0
P5
P15
P30
F
CD11c-GFP Hoechst
P0
P3
P7
P30
NbL
IPL
GCL
NFL
OPL
INL
IPL
GCL
NFL
G
P0
P3
P7
P30
%CD11c-GFP+
100
80
60
40
20
0
NbL
IPL
NFL/GCL
OPL
IPL/INL
NFL/GCL

Figure 2.

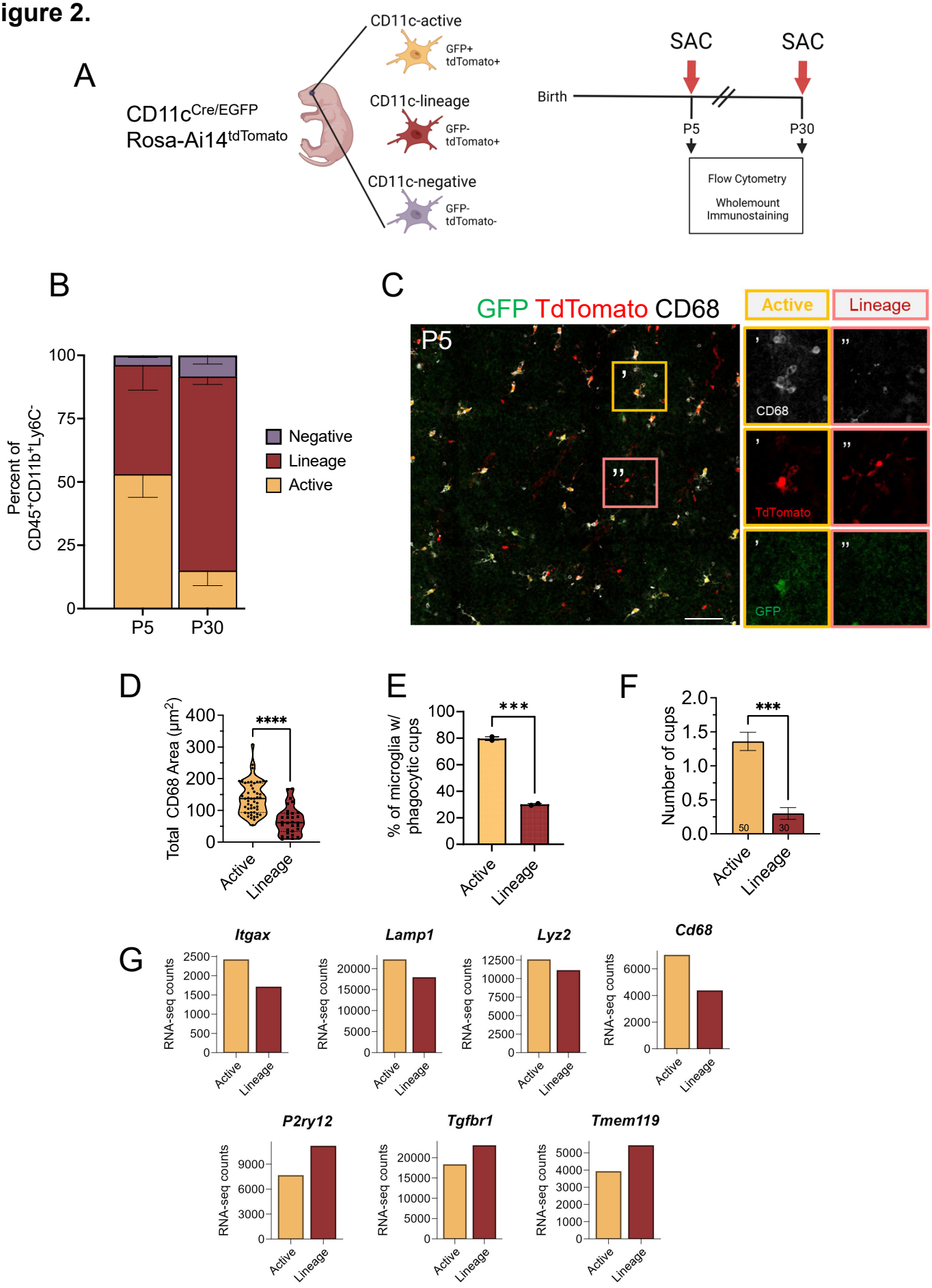
A
CD11c^Cre/EGFP
Rosa-Ai14^tdTomato
CD11c-active
GFP+
tdTomato+
CD11c-lineage
GFP-
tdTomato+
CD11c-negative
GFP-
tdTomato-
Birth
SAC
SAC
P5
P30
Flow Cytometry
Wholemount Immunostaining
B
Percent of CD45+CD11b+Ly6C-
100
75
50
25
0
P5
P30
Negative
Lineage
Active
C
GFP TdTomato CD68
Active
Lineage
P5
CD68
TdTomato
GFP
D
Total CD68 Area (µm2)
400
300
200
100
0
****
Active
Lineage
E
% of microglia w/ phagocytic cups
100
80
60
40
20
0
***
Active
Lineage
F
Number of cups
2.0
1.5
1.0
0.5
0.0
***
50
30
Active
Lineage
G
Itgax
Lamp1
Lyz2
Cd68
P2ry12
Tgfbr1
Tmem119
RNA-seq counts
Active
Lineage

Figure 3.

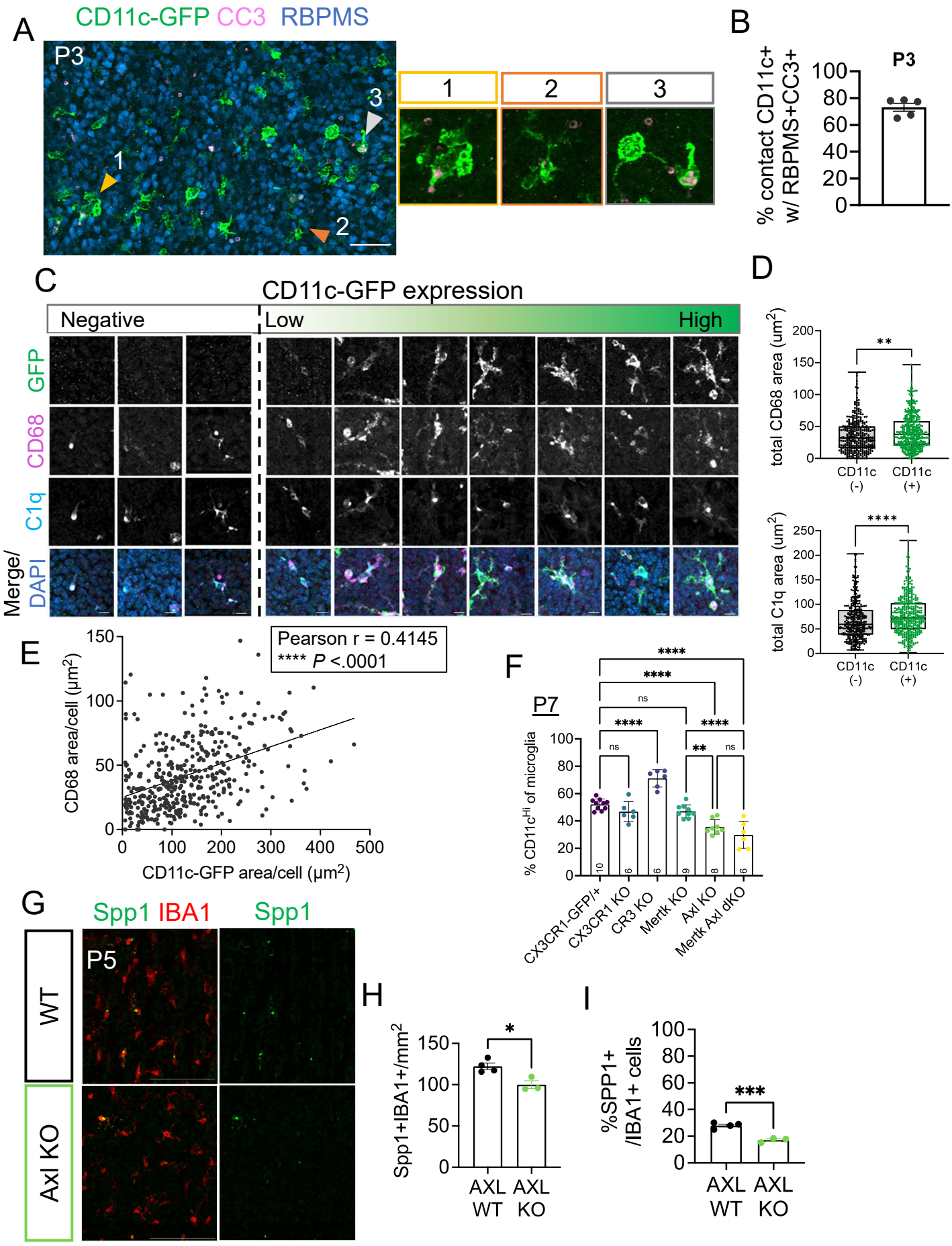
A
CD11c-GFP CC3 RBPMS
P3
1
2
3
B
P3
% contact CD11c+ w/ RBPMS+CC3+
C
CD11c-GFP expression
Negative
Low
High
GFP
CD68
C1q
Merge/ DAPI
D
total CD68 area (um2)
total C1q area (um2)
CD11c (-)
CD11c (+)
E
Pearson r = 0.4145
**** P <.0001
CD68 area/cell (µm2)
CD11c-GFP area/cell (µm2)
F
P7
% CD11cHi of microglia
CX3CR1-GFP/+
CX3CR1 KO
CR3 KO
Mertk KO
Axl KO
Mertk Axl dKO
G
Spp1 IBA1
Spp1
P5
WT
Axl KO
H
Spp1+IBA1+/mm2
AXL WT
AXL KO
I
%SPP1+ /IBA1+ cells
AXL WT
AXL KO

Figure 4.

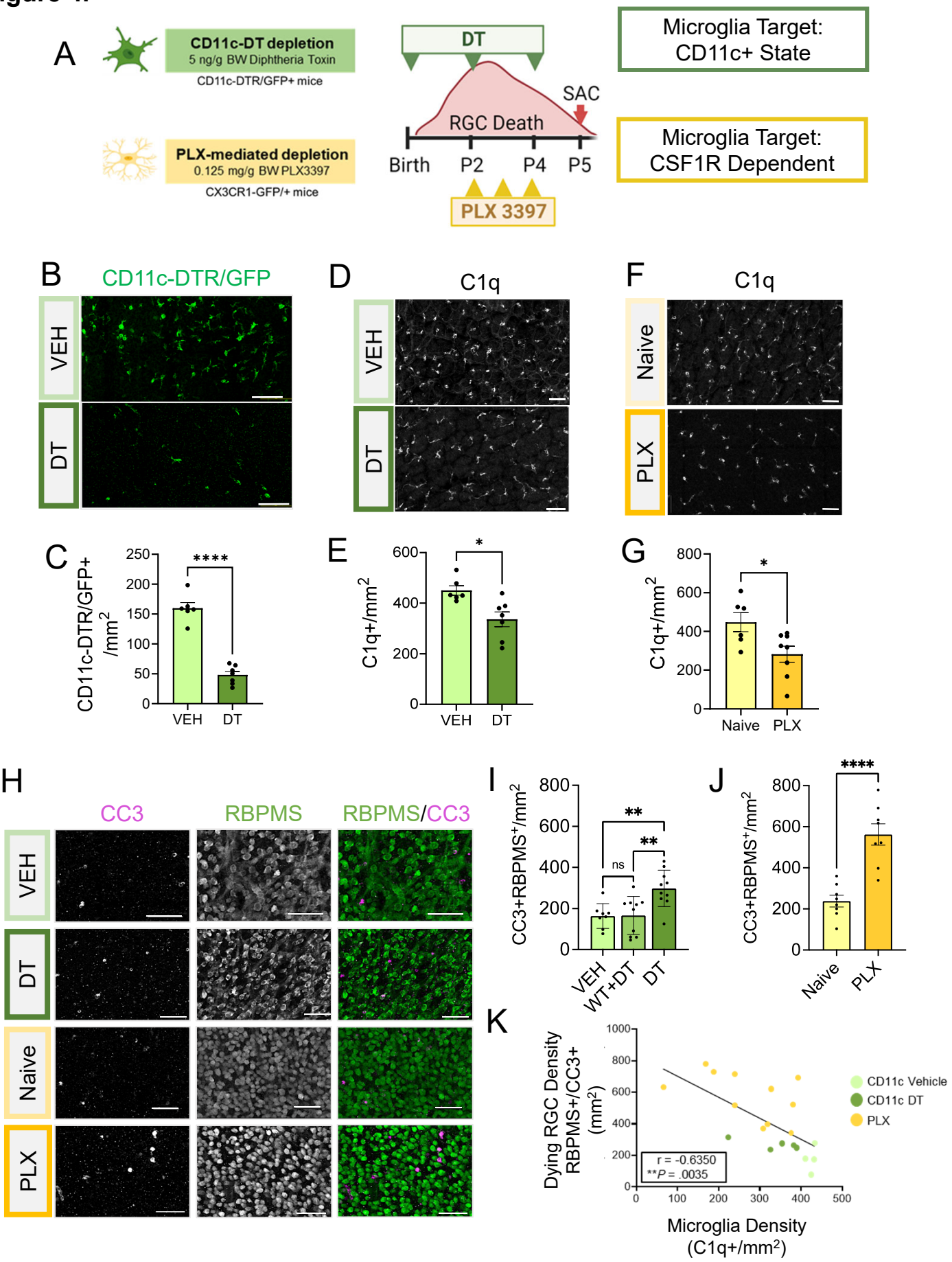
A
CD11c-DT depletion
5 ng/g BW Diphtheria Toxin
CD11c-DTR/GFP+ mice
PLX-mediated depletion
0.125 mg/g BW PLX3397
CX3CR1-GFP/+ mice
DT
SAC
RGC Death
Birth
P2
P4
P5
PLX 3397
Microglia Target: CD11c+ State
Microglia Target: CSF1R Dependent
B
CD11c-DTR/GFP
VEH
DT
D
C1q
VEH
DT
F
C1q
Naive
PLX
C
CD11c-DTR/GFP+ /mm2
****
VEH
DT
E
C1q+/mm2
*
VEH
DT
G
C1q+/mm2
*
Naive
PLX
H
CC3
RBPMS
RBPMS/CC3
VEH
DT
Naive
PLX
I
CC3+RBPMS+/mm2
**
**
ns
VEH
WT+DT
DT
J
CC3+RBPMS+/mm2
****
Naive
PLX
K
Dying RGC Density RBPMS+/CC3+ (mm2)
r = -0.6350
**P = .0035
Microglia Density (C1q+/mm2)
CD11c Vehicle
CD11c DT
PLX

Supplementary Figure S1.

A

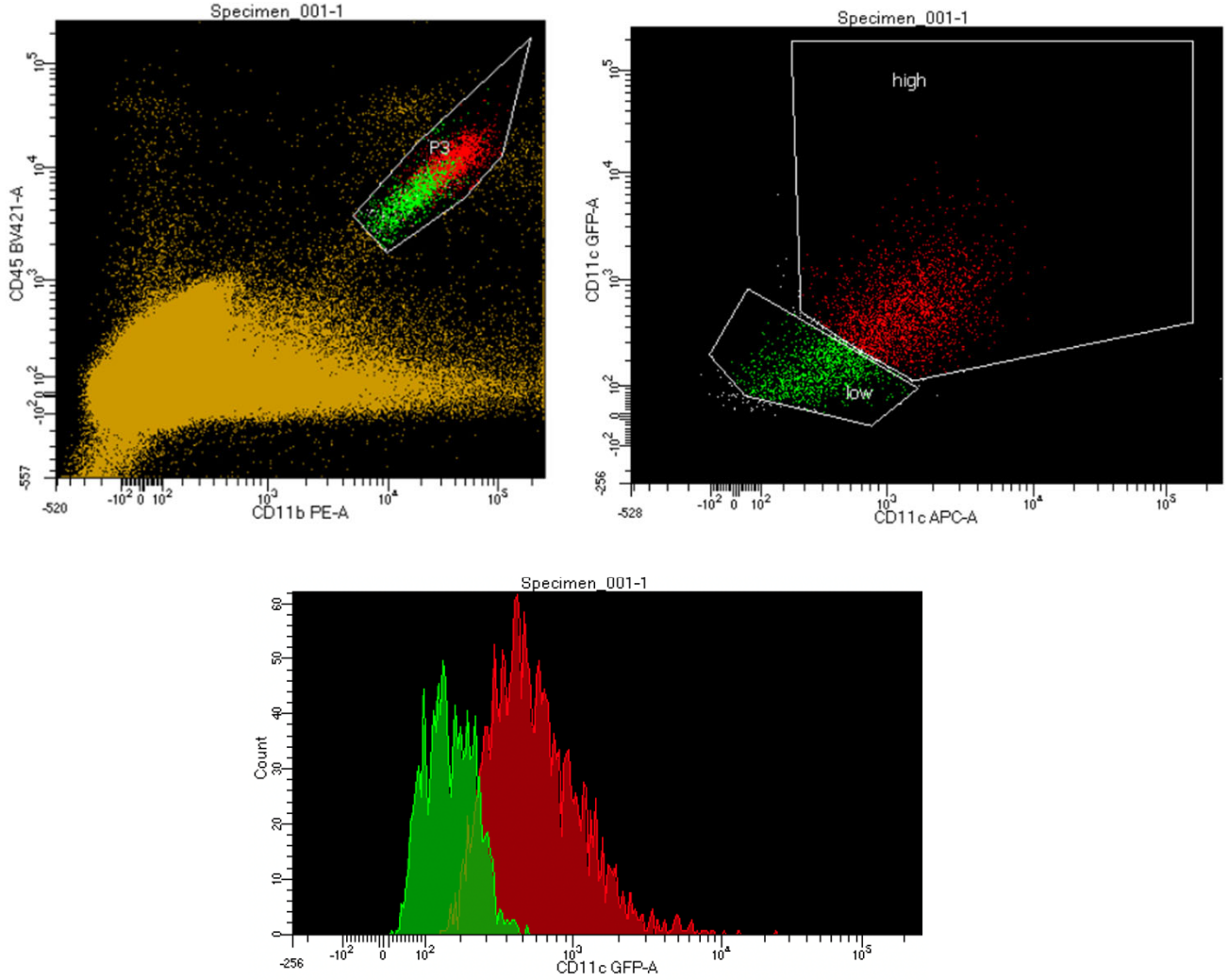

Supplementary Figure S2.

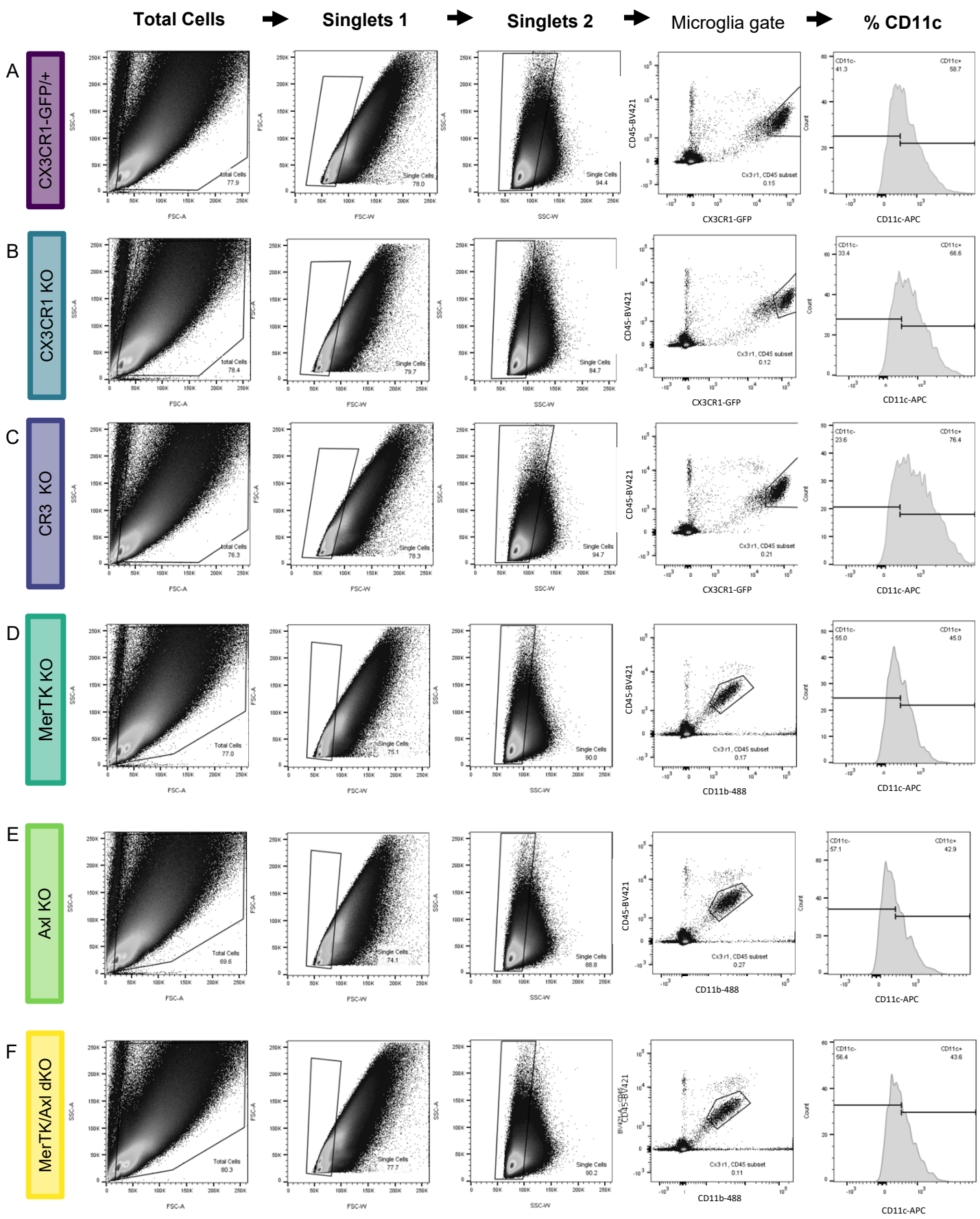
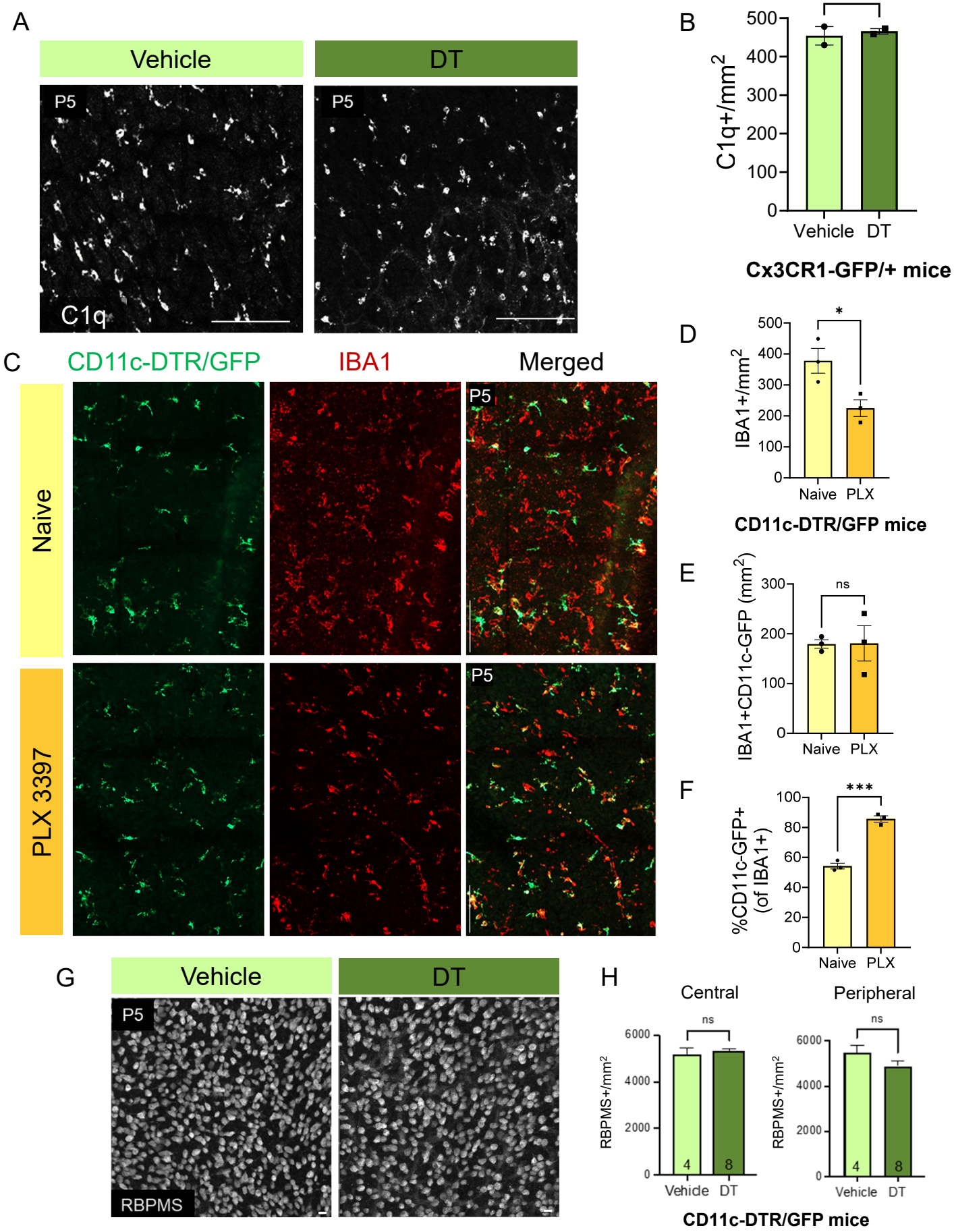
Supplementary Figure S3.